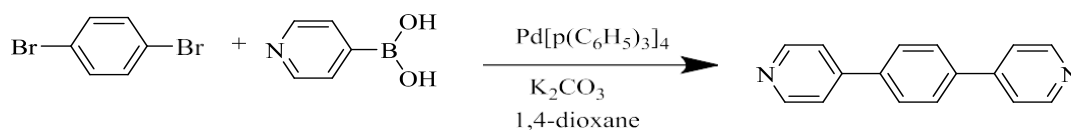

Supplementary Information

$\{[\text{Ru}(\text{bda})]_x\text{L}_y\}_n$ Cross-linked Coordination Polymers: Toward Efficient Heterogeneous Catalysis for Water Oxidation in Organic Solvent-free System

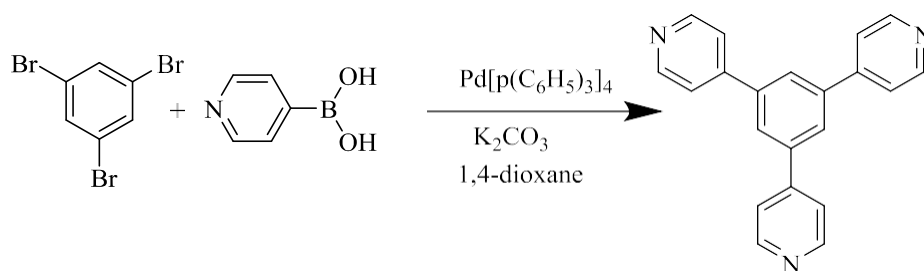
Tao Zheng and Lianwei Li*

*Hefei National Laboratory for Physical Sciences at the Microscale, Department of Chemical Physics,
University of Science and Technology of China, Hefei, Anhui 230026, China*

Preparation of multi-pyridyl ligands via Suzuki coupling

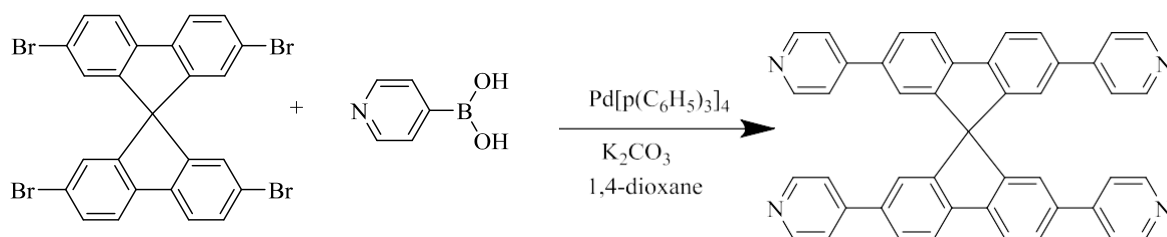


1,4-dibromobenzene (1.0 g, 4.24 mmol), 4-pyridylboronic acid (1.563 g, 12.71 mmol) and tetrakis(triphenylphosphine)-palladium(0) (293.0 mg, 0.26 mmol), were dissolved in a mixture of anhydrous 1,4-dioxane (60 mL) and K₂CO₃ solution (15 mL, 2M). The reaction mixture was heated to 110 °C and stirred for 24 hours under a nitrogen atmosphere. The mixture was cooled to room temperature, evaporated to remove 1,4-dioxane and dissolved in dichloromethane. The mixture was purified by silica gel column chromatography (eluent: ethyl acetate/methanol/triethylamine, 100/5/1, v/v/v). The product was evaporated to remove dichloromethane and dried in vacuum for 12 h at room temperature to give 1,4-bis(4-pyridyl)benzene (Yield:80%).



1,3,5-tribromo-benzen (1.0 g, 3.17 mmol), 4-pyridylboronic acid (2.342 g, 19.05 mmol) and tetrakis(triphenylphosphine)-palladium(0) (550.0 mg, 0.48 mmol), were dissolved in a mixture of anhydrous 1,4-dioxane (60 mL) and K₂CO₃ solution (15 mL, 2M). The reaction mixture was heated to 110 °C and stirred for 24 hours under a nitrogen atmosphere. The mixture was cooled to room

temperature, evaporated to remove 1,4-dioxane and dissolved in dichloromethane. The mixture was purified by silica gel column chromatography (eluent: ethyl acetate/methanol/triethylamine, 100/5/1, v/v/v). The product was evaporated to remove dichloromethane and dried in vacuum for 12 h at room temperature to give 1,3,5-tri(4-pyridyl)benzene (Yield:75%).



2,2',7,7'-tetrabromo-9,9'-spirobifluorene (1.0 g, 1.54 mmol), 4-pyridylboronic acid (1.167 g, 9.21 mmol) and tetrakis(triphenylphosphine)-palladium(0) (215.1 mg, 0.19 mmol), were dissolved in a mixture of anhydrous 1,4-dioxane (60 mL) and Na₂CO₃ solution (15 mL, 2M). The reaction mixture was heated to 110 °C and stirred for 24 hours under a nitrogen atmosphere. The mixture was cooled to room temperature, evaporated to remove 1,4-dioxane and give solid mixture. The mixture was dissolved in dichloromethane, filtered to get filtrate and the filtrate was evaporated to get product. The product was washed by ice methanol and dried in vacuum for 12 h at room temperature to give 2,2',7,7'-tetra(4-pyridyl)-9,9'-spirobifluorene (Yield:67%).

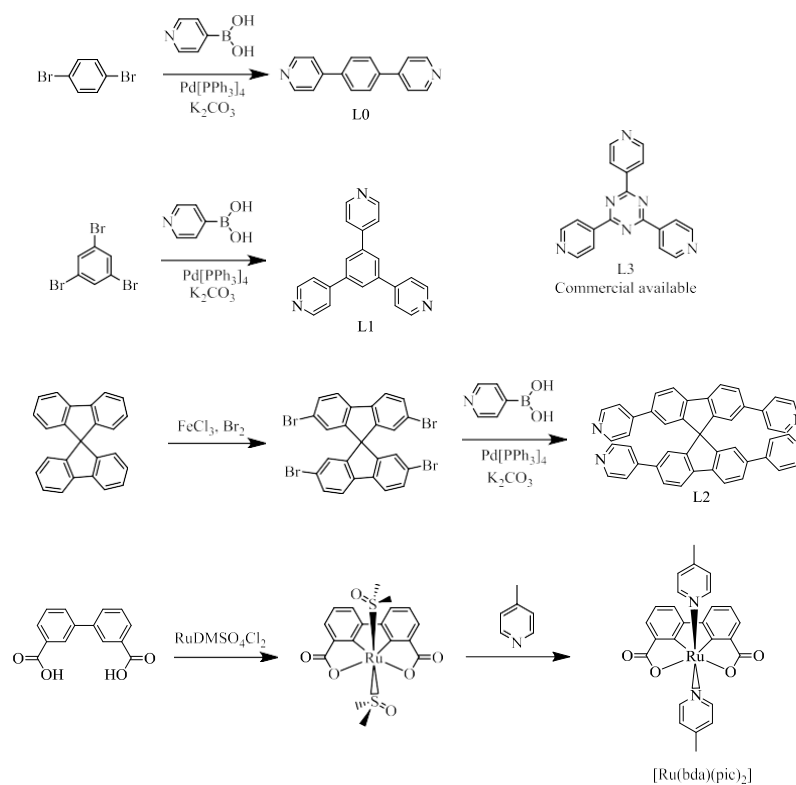
Table S1. Experimental conditions of CCP water suspensions used for kinetics study.

	[Ru(bda)pic ₂]	LCP	CCP1	CCP2	CCP3
^a Injection concentration/ (μg/mL)	25, 50, 100, 200	200, 400, 1000	200, 400, 1000	200, 400, 1000	50, 100, 200, 400
^b m _{Ru} /μg	4.8, 9.6, 19.2, 38.4	31.6, 63.2, 158	34.4, 68.8, 172	32.2, 64.4, 161	9.9, 17.8, 35.6, 71.2
^c C _{Ru} /μM	4.75, 9.50, 19.0, 38.0	31.3, 62.6, 156.4	34.1, 68.1, 170.5	31.9, 63.8, 159.5	8.82, 17.63, 35.25, 70.5

^a: Injection concentration represents the mass concentration of CCP in the injected water suspension (0.5 mL).

^b: m_{Ru} represents the calculated absolute mass of Ru element in the injected water suspension (0.5 mL) based on ICP-MS results.

^c: C_{Ru} represents the calculated molar concentration of Ru in the final water suspension (10 mL) used in catalysis.

**Figure S1.** Schematic synthesis of intermediate products, ligands L0-L3 and [Ru(bda)(pic)₂].

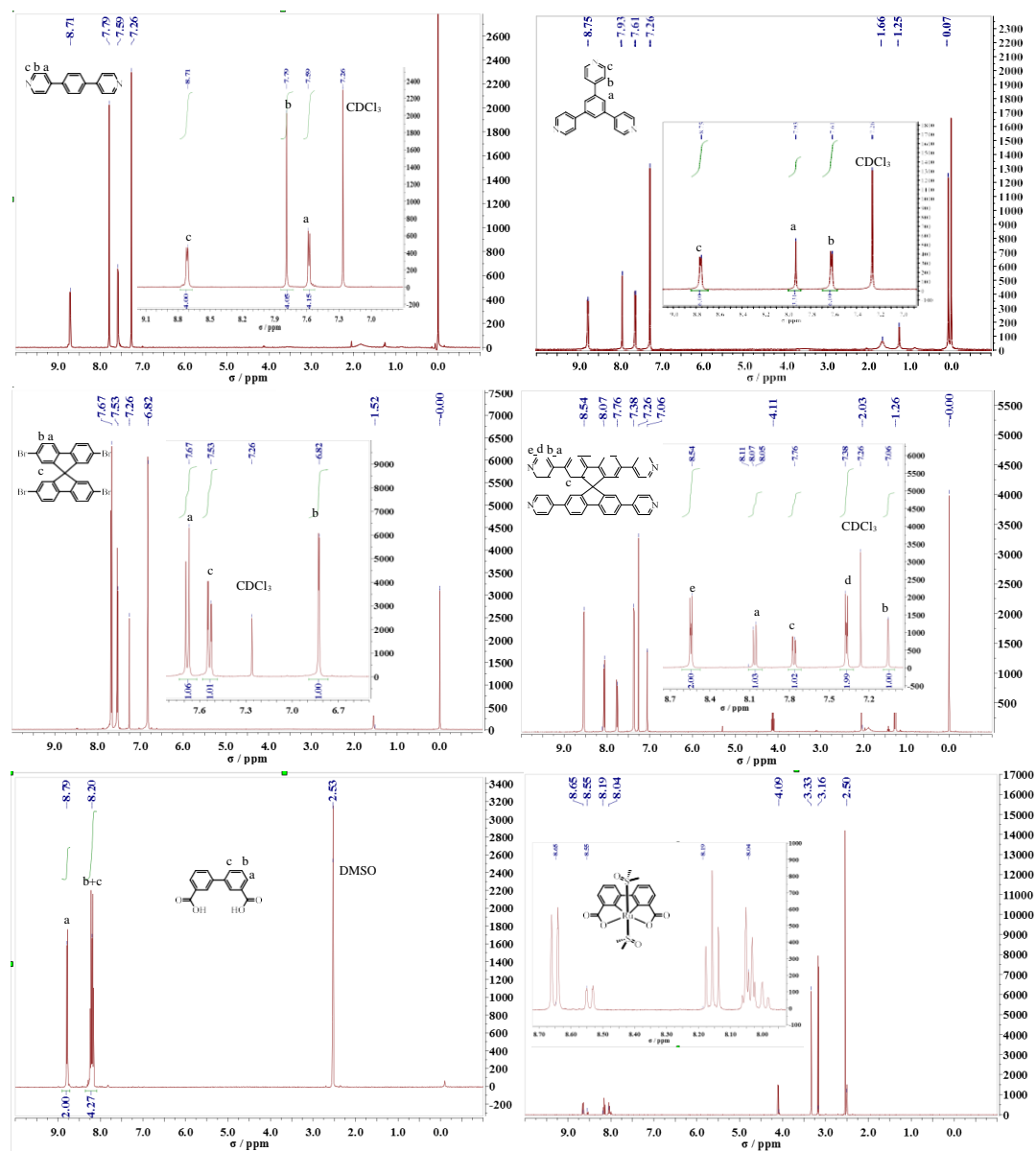


Figure S2. NMR spectra of multi-pyridyl ligands and other intermediate products.



Figure S3. (a) and (b) Digital photographs of reaction mixture (**CCP3**) at $t = 1$ h and $t = 24$ h. (c) and (d) Digital photographs of reaction mixture (**CCP3**) before and after centrifugation.



Figure S4. (a) Digital photograph of reaction vials containing CAN for catalysis study. (b) Digital photograph of CCP water suspensions with a polymer concentration of 1.0 g/L.

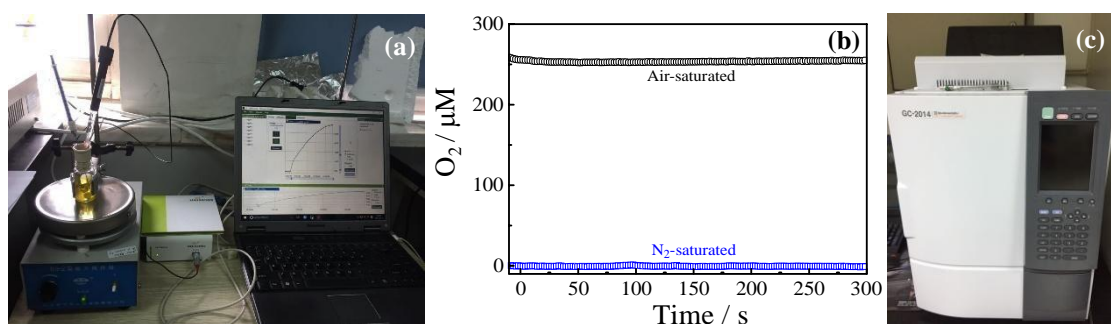


Figure S5. (a) Digital photographs of reaction vial and oxygen sensor system. (b) Calibration curves monitored by oxygen sensor for kinetics study. (c) Digital photograph of GC system (Shidadzu).

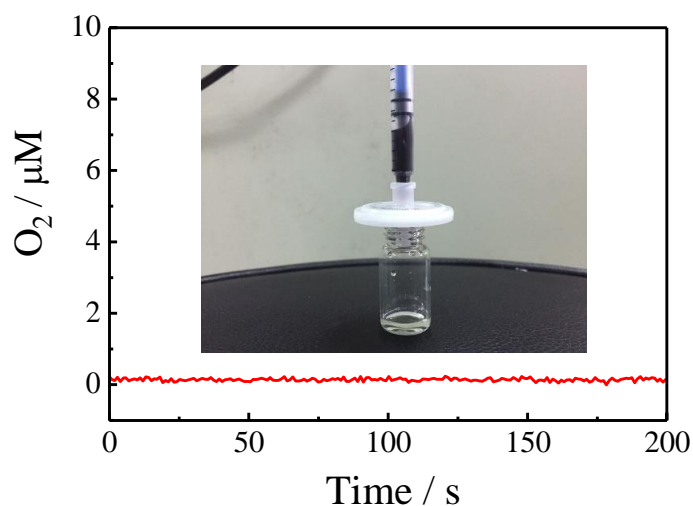


Figure S6. Plot of oxygen evolution versus time by using the filtrate of CCP3 suspension (1.0 mg/mL) as catalyst solution.

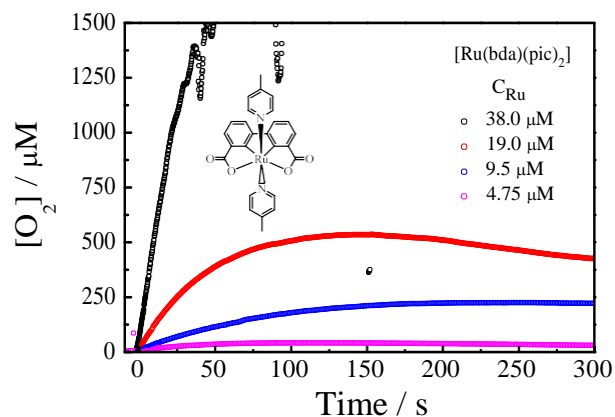


Figure S7. Reaction time (t) dependence of oxygen concentration ($[O_2]$) by using the reference $[Ru(bda)(pic)_2]$ as WOCs ($[Ce^{IV}] = 100 \text{ mM}$, $pH = 1.0$).

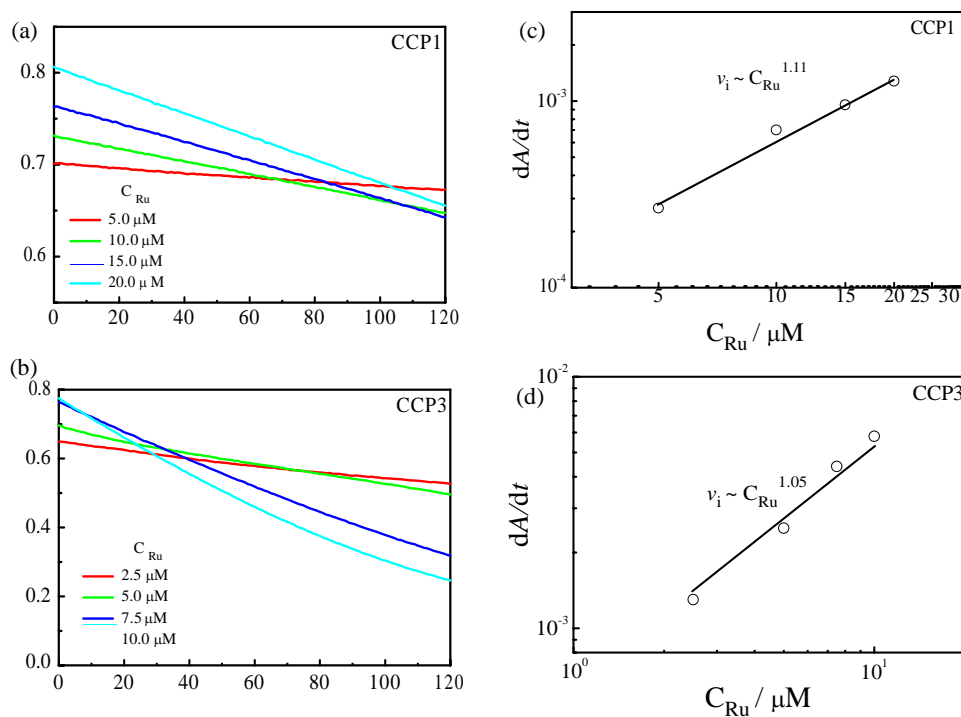


Figure S8. (a) and (b) Reaction time (t) dependence of Ce^{IV} absorbance decay at 360 nm for **CCP1** and **CCP3**, where $[Ce^{IV}] = 1.12 \text{ mM}$. (c) and (d) Catalyst concentration (C_{Ru}) dependence of initial reaction rate (dA/dt) for **CCP1** and **CCP3**, where $[Ce^{IV}] = 1.12 \text{ mM}$.

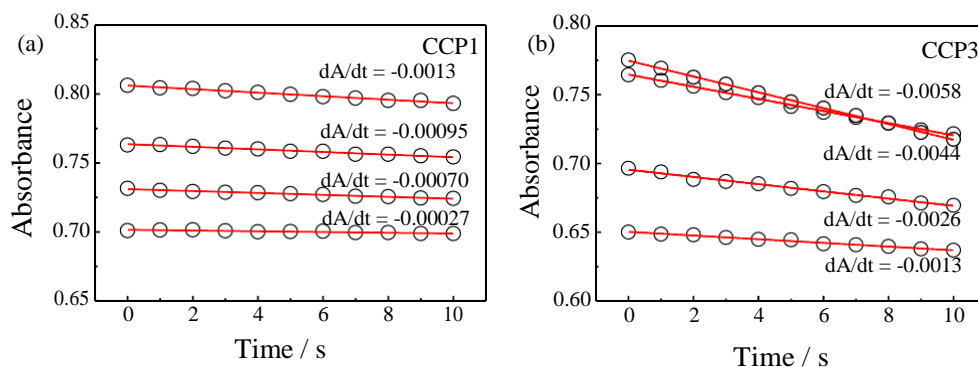
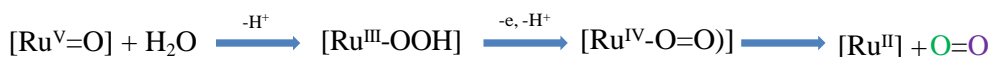


Figure S9. Linear fitting of experimental data obtained within the first few seconds in Figures S8.

Mechanism 1: single-site water nucleophilic attack



Mechanism 2: interaction of two metal oxide units

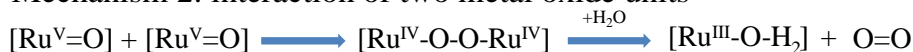


Figure S10. Potential mechanistic pathways for water oxidation catalysis: 1) single-site water nucleophilic attack; 2) interaction of two metal oxide units.

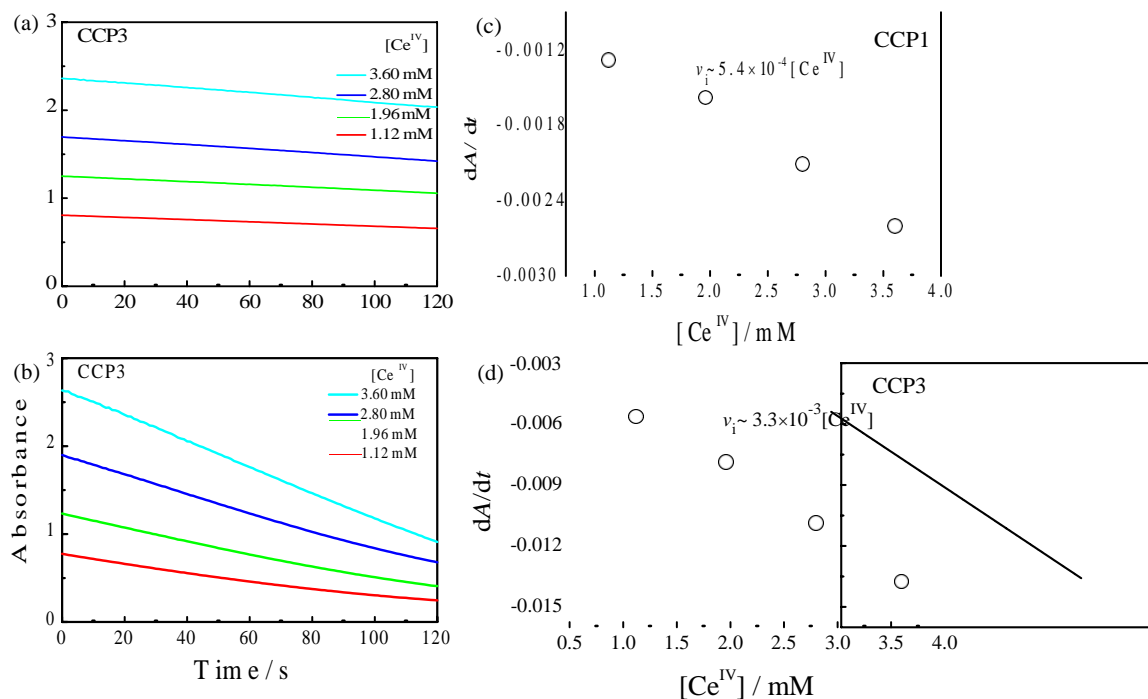


Figure S11. (a) and (b) Reaction time (t) dependence of Ce^{IV} absorbance decay at 360 nm for **CCP1** and **CCP3**, where $C_{\text{Ru}} = 20 \mu\text{M}$ (**CCP1**) and $10 \mu\text{M}$ (**CCP3**). (c) and (d) Oxidant concentration ($[\text{Ce}^{\text{IV}}]$) dependence of initial reaction rate (dA/dt) for **CCP1** and **CCP3**, where $C_{\text{Ru}} = 20 \mu\text{M}$ (**CCP1**) and $10 \mu\text{M}$ (**CCP3**).

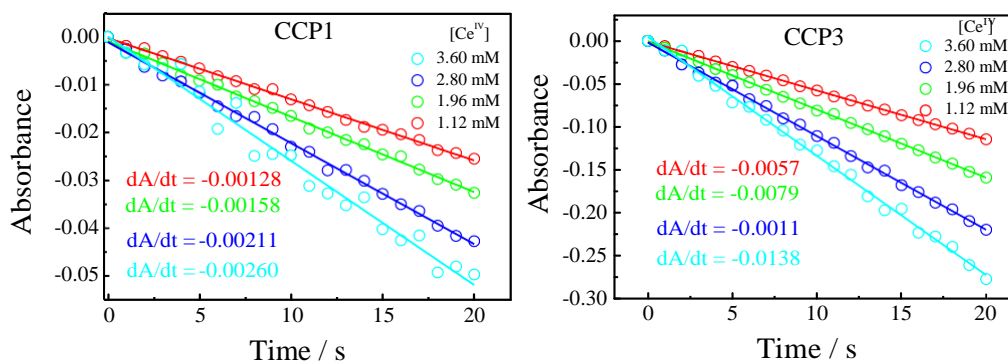


Figure S12. Linear fitting of experimental data obtained within the first few seconds in Figures S11.

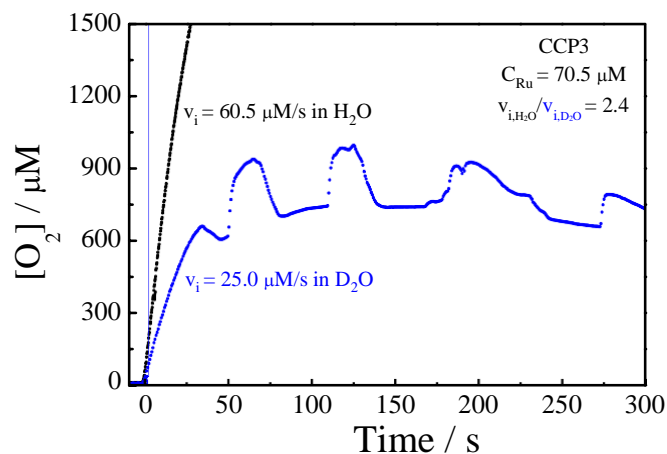


Figure S13. Reaction time (t) dependence of oxygen concentration ($[O_2]$) by using CCP3 as WOCs in H_2O and D_2O , where $[Ce^{IV}] = 100 \text{ mM}$ and $\text{pH} = 1.0$ (HNO_3).

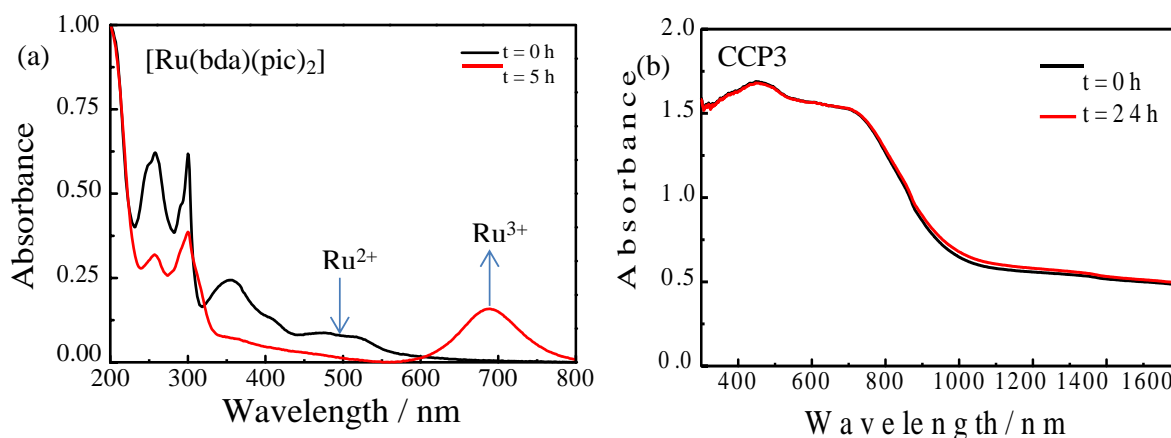


Figure S14. (a) UV-vis spectra of $[Ru(bda)(pic)_2]$ stock solution before and after stirring for 5 h. (b) Diffusion reflectance UV-vis spectra of CCP3 before and after stirring for 24 h.

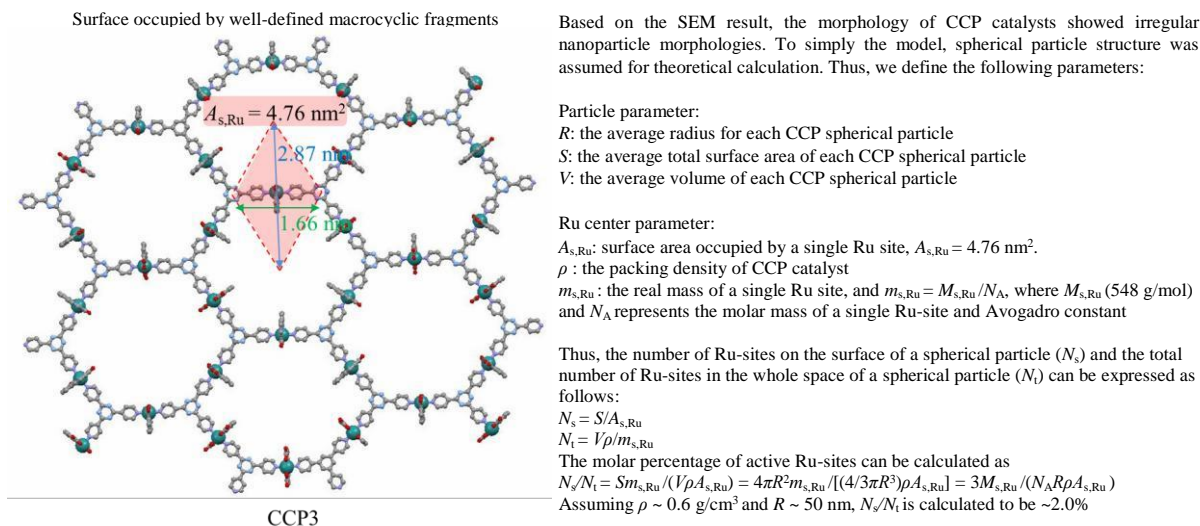


Figure S15. Calculation of the number densities of active Ru sites located at the outermost layer of porous framework for **CCP3**.

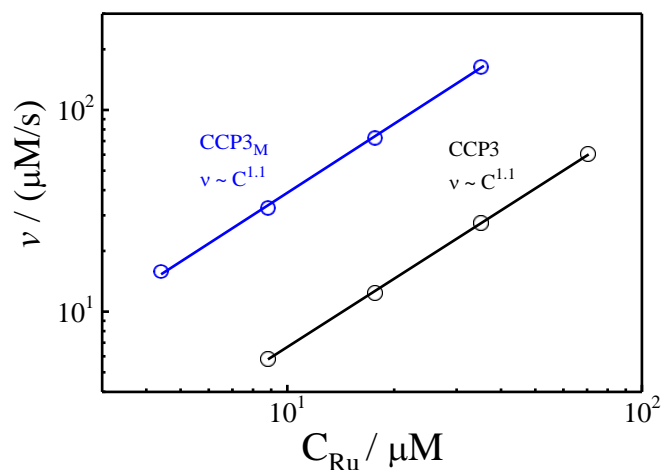


Figure S16. Catalyst concentration (C_{Ru}) dependence of initial oxygen evolution rate (v_i) in log-scale coordinate for **CCP3** and **CCP3_M**, where C_{Ru} represents the molar concentration of Ru in suspension used in catalysis reaction.

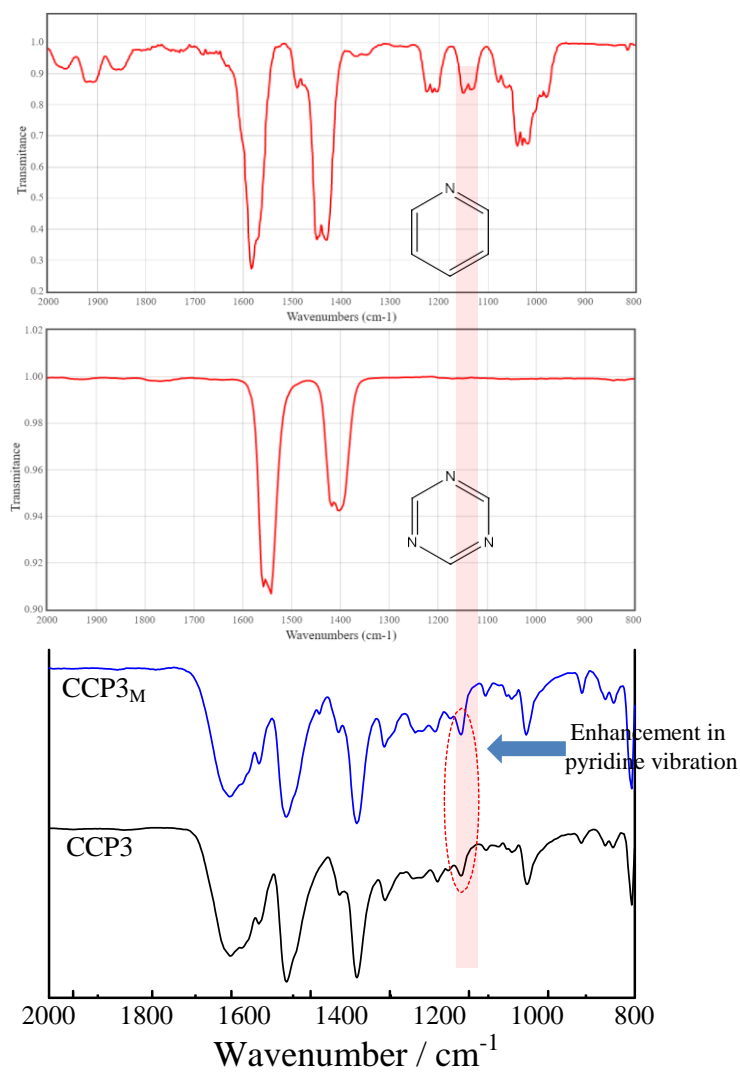


Figure S17. FTIR spectra of **CCP3** and **CCP3_M**.

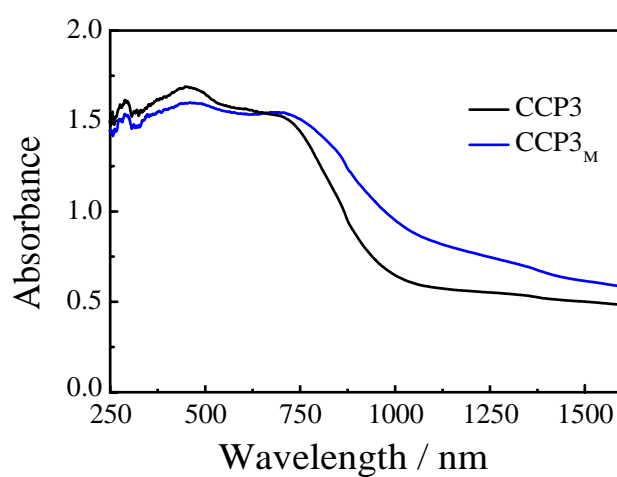


Figure S18. (b) Diffusion reflectance UV-vis spectra of **CCP3** and **CCP3_M**.

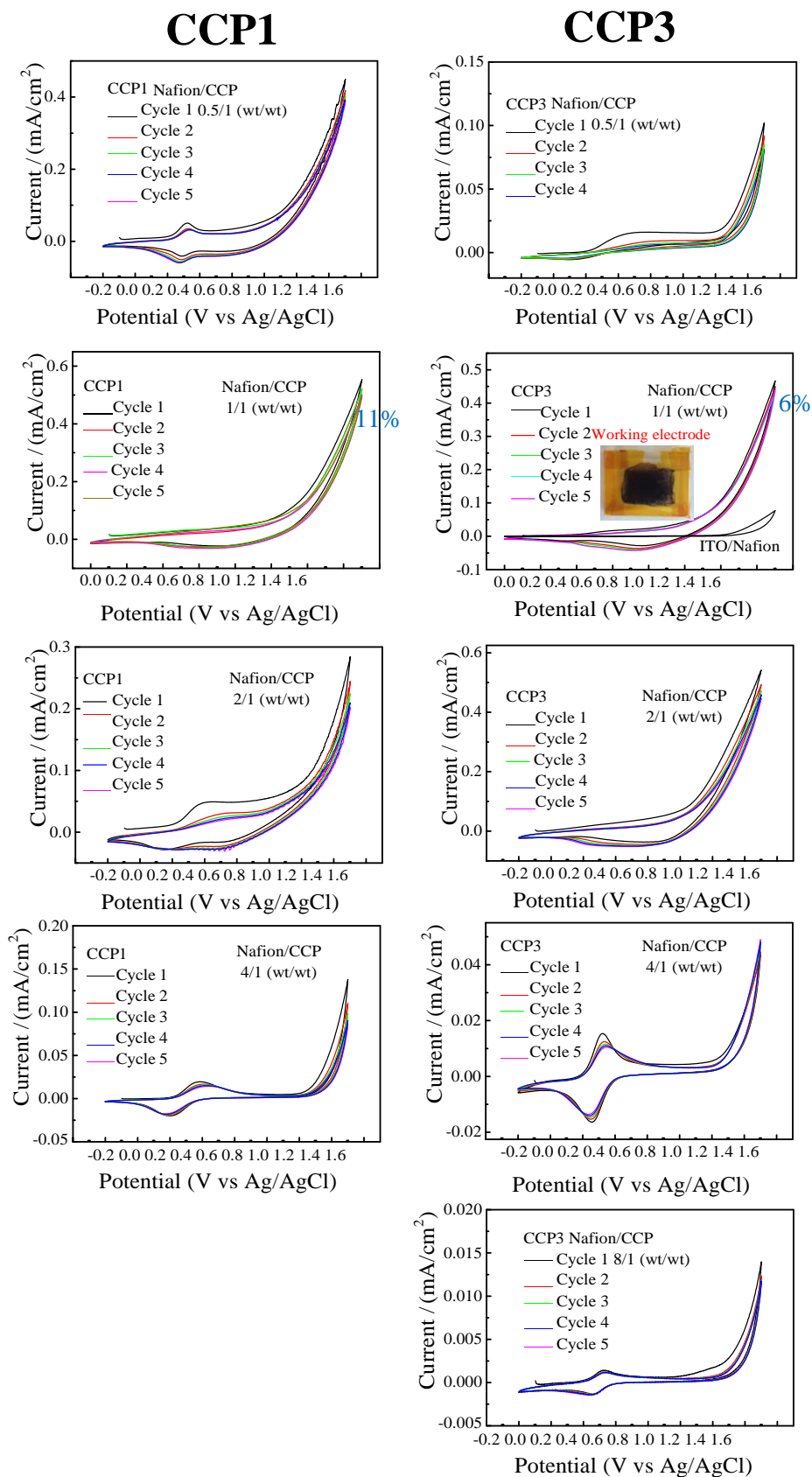


Figure S19. (a) Repetitive cyclic voltammograms (CVs) for **CCP/Nafion/ITO** electrodes at pH = 8.0 up to 1.50 V (100 mV/s), where mass ratio of **CCP/Nafion** was varied.

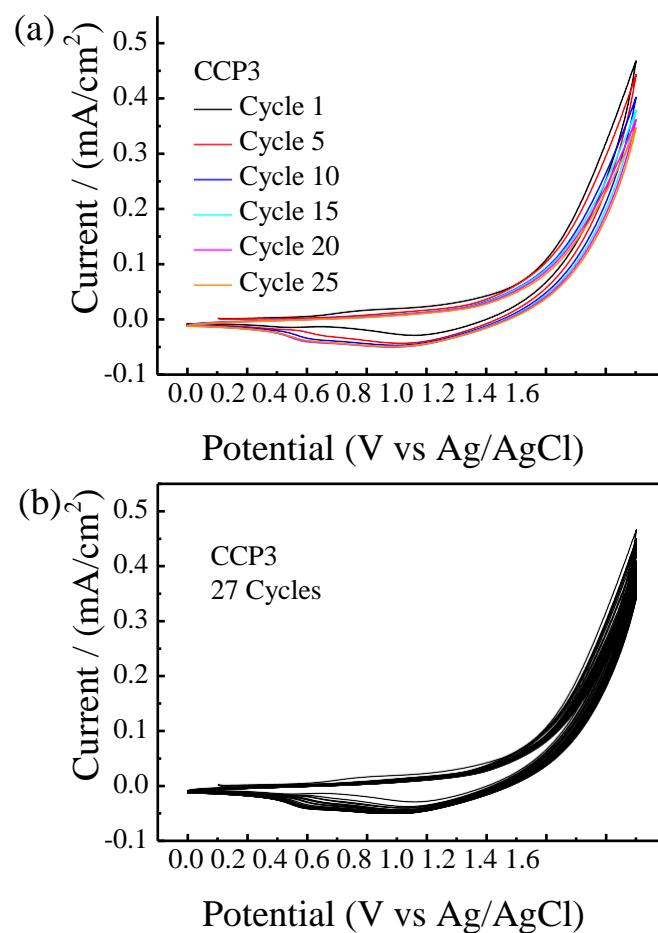


Figure S20. (a) and (b) Repetitive cyclic voltammograms (CVs) for CCP3/Nafion/ITO electrodes at pH = 8.0 up to 1.50 V (100 mV/s) for 27 cycles.